Design and experiment of the ditching device for wheat seeders capable of ditching sloped drainage furrows in rice-wheat rotation areas

Quanyu Wang[1,2], Ming Peng[1,2], Jin He[1,2*], Caiyun Lu[1,2], Chao Wang[1,2], Zhenwei Tong[1,2]

(1. *College of Engineering, China Agricultural University, Beijing 100083, China*;
2. *Scientific Observing and Experiment Station of Arable Land Conservation (North Hebei), Ministry of Agricultural and Rural Affairs, Beijing 100083, China*)

Abstract: To solve the problem of field waterlogging during wheat sowing in rice-wheat rotation areas, which causes sticky and wet soil, thus affecting the growth of wheat, this paper proposed a sloped ditching method based on laser alignment technology, and designed a combined ditching device with a front ditching shovel (FDS) and a rear ditching plow (RDP) to create sloped drainage furrows when sowing wheat. The key factors affecting the performance of RDP and value ranges were determined through theoretical analysis. Through discrete element method (DEM) simulation, the influence of different structural parameter combinations on slope stability was studied, and the optimal parameter combination was determined as the soil lifting angle of 50°, the minimum element angle of 35°, and the maximum element angle of 40°. The field test showed that the ditching device can effectively create sloped trapezoidal drainage furrows. The slope stability coefficient and slope accuracy coefficient were both greater than 85%, which meets the requirements of drainage. This paper provides a new ditching method and theoretical basis for the development of a sowing and ditching combined machine in rice stubble fields.

Keywords: rice-wheat rotation, laser, wheat seeder, sloped drainage furrow, discrete element method
DOI: 10.25165/j.ijabe.20251801.8934

Citation: Wang Q Y, Peng M, He J, Lu C Y, Wang C, Tong Z W. Design and experiment of the ditching device for wheat seeders capable of ditching sloped drainage furrows in rice-wheat rotation areas. Int J Agric & Biol Eng, 2025; 18(1): 154–164.

1 Introduction

The rotation of rice and wheat in the rice-planting areas in the middle and lower reaches of the Yangtze River in China plays an important role in ensuring China's food security[1]. In the above-mentioned areas, rainfall is heavy during the wheat sowing period, so field water accumulates easily and is difficult to drain, resulting in high soil moisture[2]. The wheat roots staying in sticky and wet soil for a long period will have a negative impact on the respiratory function of the roots, which is harmful to the growth and yield of wheat. Research shows that ditching for drainage is beneficial for maintaining and increasing the yield of rice and wheat[3]. Therefore, it is necessary to ditch drainage furrows during wheat sowing to accelerate the drainage of waterlogging and reduce soil water content.

The operation method of first rotary tilling and sowing, and then ditching drainage furrows has the disadvantages of high labor intensity, increased production costs, and increased soil compaction. The combined operation machines with the function of sowing and ditching can reduce soil compaction, shorten agricultural time intervals, and improve economic benefits. Therefore it has become the mainstream type of machinery for wheat sowing in rice stubble fields[4]. Zhu et al.[5] symmetrically positioned furrow openers on both sides of a no-till wheat seeder, facilitating simultaneous furrow formation during wheat sowing. Hu et al.[6] developed a reduced-tillage wheat planter for rice stubble fields, incorporating a double-wing moldboard opener. The planter achieved an average furrow depth of 175 mm and a width of 238 mm, effectively meeting the drainage requirements. Zheng et al.[7] employed a combination of disc ditching components and a furrow finishing device to form drainage furrows in the cultivated area, with both furrow width and depth stability exceeding 80%. In the middle and lower reaches of the Yangtze River, it is essential to create drainage furrows on both sides of the seedbed during the sowing of rapeseed to mitigate the risk of waterlogging and ensure optimal crop growth[8]. The rapeseed direct seeder is the predominant equipment for sowing rapeseed in the middle and lower reaches of the Yangtze River, with the furrow ditching device serving as a critical component for the simultaneous formation of drainage furrows during the sowing process. Liu et al.[9] developed a furrow ditching system for rapeseed combined seeding machines, which consists of a moldboard plow and a composite boat-shaped opener. Under various operating conditions, the system demonstrated furrow width and depth stability coefficients greater than 90%. Liu proposed an active rotary cutting furrow opener, where the furrow cutting disc and soil distribution plate work together to create drainage furrows and cover the seedbed surface[10]. The stability coefficients for both furrow depth and width were found to exceed 90%. Zhang et al.[11] developed a rapeseed direct seeder with a furrow opener and shallow rotary device, in which the furrow cutting disc and soil shaping components work together to create drainage furrows. This development significantly improved the stability of the furrow ditching operation, with both furrow depth and width stability coefficients exceeding 85%. Wang et al.[12] designed a driven-type

Received date: 2024-03-19 **Accepted date:** 2025-01-05
Biographies: Quanyu Wang, PhD candidate, research interest: conservation tillage and equipment, Email: wangquanyu@cau.edu.cn; **Ming Peng**, MS, research interest: conservation tillage and equipment, Email: 874084766@qq.com; **Caiyun Lu**, PhD, Associate Professor, research interest: conservation tillage and equipment, Email: lucaiyun@cau.edu.cn; **Chao Wang**, PhD, Associate Professor, research interest: conservation tillage and equipment, Email: superc@cau.edu.cn; **Zhenwei Tong**, PhD candidate, research interest: conservation tillage and equipment, Email: tongzhenwei917@163.com.
***Corresponding author: Jin He**, PhD, Professor, research interest: conservation tillage and equipment. College of Engineering, China Agriculture University, No.17, Qinghua East Road, Haidian District, Beijing 100083, China. Tel: +86-10-62737300, Email: hejin@cau.edu.cn.

paddle-like furrow opener for direct seeding of rapeseed. This device can simultaneously perform high-speed furrow formation and ensure uniform soil coverage over the seedbed surface. The average furrow depth ranged from 169.1 to 188.6 mm, with the furrow depth stability coefficient ranging from 92.5% to 95.6%. Although the studies mentioned above enable the simultaneous formation of drainage furrows during sowing, which helps alleviate waterlogging in the field, the effectiveness of the drainage is limited. This limitation arises from the lack of slope in the furrows, as the drainage process depends solely on the elevation differences in the terrain.

Laser land leveling technology significantly enhances surface flatness, thereby promoting the efficient utilization of water and fertilizers[13,14]. Numerous studies have been conducted to improve the control accuracy and stability of land levelers, while also focusing on reducing fuel consumption[15-18]. Furthermore, the laser measurement method has found extensive applications in assessing surface characteristics after tillage and in monitoring soil erosion processes. Zhang et al.[19] utilized laser scanning technology to study the evolution characteristics and patterns of surface roughness during water erosion processes on sloped land. Wang et al.[20] developed a furrow measurement system based on the laser triangulation method, with an interactive interface that can display furrow roughness, furrow width, furrow depth, and stability variation coefficients in real time. The multi-sensor seeding depth monitoring system, consisting of a laser sensor, ultrasonic sensor, and angle sensor, improves the accuracy and reliability of the seeding depth monitoring system[21]. In summary, the application of laser measurement technology in farmland surface leveling and terrain feature acquisition has made significant progress. This study applies laser measurement technology to the furrow ditching operation of no-till wheat sowing in rice stubble fields, aiming to achieve precise control of the furrow slope.

The discrete element method is extensively applied in the study of furrow resistance reduction and moldboard surface optimization, as it accurately simulates the interaction between the soil and the working components[22,23]. Zhang et al.[24] conducted discrete element method (DEM) simulations, using moldboard surface parameters and operating speed as experimental factors, with traction resistance as the evaluation index. They developed a moldboard surface optimization model that effectively reduced ditching resistance. Liu et al.[25] employed a combination of differential geometry theory and DEM simulations to optimize the soil-contact surfaces of a boat-shaped furrow opener. Liu employed the DEM to investigate the interaction mechanism between the furrow opener and soil, leading to the identification of an optimal combination of blade structural parameters[10]. Based on the DEM simulations, Wang et al.[26] conducted both single-factor and optimization analyses on the structural parameters of a paddle-like furrow opener. The optimized design resulted in furrow depth and width stability coefficients exceeding 90%. This study employs DEM simulations to model the ditching process and optimize the critical structural parameters of the ditching plow, with the goal of achieving enhanced soil handling efficiency and performance improvement.

In order to accelerate the drainage of field waterlogging and reduce soil water content, and in combination with the regional agronomic planting requirements, this paper developed a wheat seeder that can ditch sloped furrows suitable in rice-wheat rotation areas. Based on the laser alignment system, a combined ditching device with a front shovel and a rear plow was designed. This device can ditch drainage ditches with certain slopes while performing wheat sowing operations, thereby creating better soil conditions for the emergence and growth of wheat.

2 Overall structure and working principle

2.1 Structure of the wheat seeder with sloped ditching function

As shown in Figure 1, the wheat seeder capable of ditching sloped drainage furrows mainly consists of a front ditch shovel (FDS), a soil deflector, a spiral soil leveler, a laser receiver, a vibration damping and stabilization system, a rear ditch plow (RDP), etc. According to the agronomic requirements for wheat planting in the rice-wheat rotation areas in China, the machine adopts the ditching method with a front shovel and a rear plow. When sowing wheat in rice stubble fields, it simultaneously ditches drainage furrows with slopes to accelerate the drainage of field water. The main technical parameters of the machine are listed in Table 1.

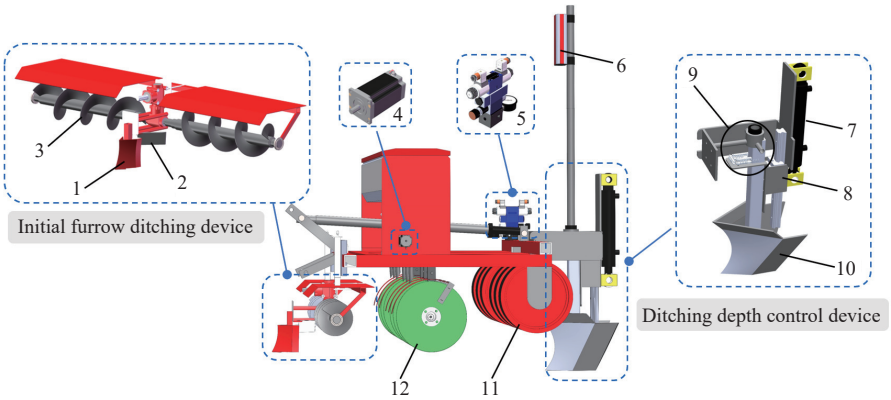

1. Front ditching shovel 2. Soil deflector 3. Spiral soil leveler 4. Stepper motor 5. Solenoid valve group 6. Laser receiver 7. Hydraulic cylinder 8. Slide rail slider 9.Vibration damping and stabilization system 10. Rear ditching plow 11. Compress wheel 12. Double disc opener

Figure 1 Wheat seeder with ditching function

2.2 Working principle

The wheat seeder is connected to the tractor through a three-point linkage. The tractor's PTO provides power to the spiral soil leveler, and the battery supplies power to the electric-driven seeding system. The FDS first creates an initial furrow, providing a foundation for the excavation of a sloped drainage furrow. The laser alignment system consists of a laser transmitter, a laser receiver, a laser controller, a solenoid valve group, and a hydraulic cylinder, as

shown in Figure 2. The types and technical parameters of each component are listed in Table 2.

Table 1 Technical parameters of the wheat seeder

Parameter	Value
Whole machine operation width/mm	1662
Supporting power/kW	≥60
Number of sowing rows	6
Operating speed/m·s^{-1}	0.5-1.8
Maximum depth of drainage furrow/mm	350
Maximum width of drainage furrow/mm	380
Maximum theoretical slope value of drainage furrow/(°)	0.345

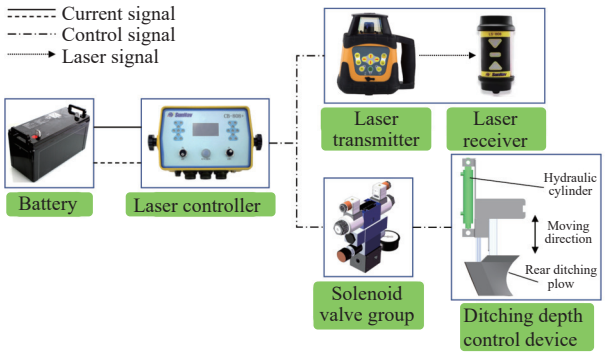

Figure 2 Composition of laser alignment system

Table 2 Technical parameters of laser alignment system components

Components	Type	Technical parameters
Laser transmitter	TC-808-P	Self-leveling range: ±5° Self-leveling accuracy: horizontal ±10″, vertical ±15″ Effective transmission distance: 500 m
Laser receiver	LR-505	Voltage input: 10-30 V DC Detection window: 190 mm Receiving angle range: 360°
Laser controller	CB-808+	Voltage input: 9-36 V DC Leveling accuracy: ±2 cm Operating temperature: –4°C to 7°C
Two-position four-way solenoid directional valve	WE6	Operating voltage: 12 V Operating pressure: 0-60 MPa Flow rate: 60 L·min^{-1}
Two-way flow control valve	2FRM	Rated flow: 15 L·min^{-1} Operating pressure: 0-21 MPa Opening pressure: 0.1 MPa
Stacked relief valve	ZDB	Maximum operating pressure: 0-31.5 MPa Flow range: 0-60 L·min^{-1}

The laser plane generated by the laser transmitter with a slope is taken as the reference plane for sloped ditching operations. The laser receiver detects the position of the laser plane with a certain slope, and then calculates the positional deviation of the RDP relative to the slope reference plane. After converting the positional deviation signal into an electrical signal, it is transmitted to the laser controller. The controller processes the signal and sends commands to the hydraulic system, which adjusts the entry depth of the RDP, thereby achieving sloped ditching. Figure 3 shows the working principle of the wheat seeder capable of ditching sloped drainage furrows. The vibration damping and stabilization system reduces the impact of vibration on the operation accuracy and improves the stability of the ditching operation.

In rice-wheat rotation areas, the soil tends to be heavy and compacted, and the vibrations generated by the high-speed rotating shaft during active ditching will significantly reduce the accuracy of the laser alignment system. In contrast, passive ditching produces smaller vibrations, which are beneficial for maintaining the relative integrity of the furrow shape. Therefore, the passive combined trenching method is adopted in this paper. The ditching components consist of an FDS and RDP, which are arranged at the front and rear of the wheat seeder, respectively. The FDS creates the initial furrow, and the RDP further operates under the action of the hydraulic adjustment system to form a complete furrow, ultimately finishing a sloped drainage furrow. The vertical height relationship between the FDS and the RDP affects the slope accuracy and operating resistance. As shown in Figure 4, both situations Ⅰ and Ⅲ will reduce the operational accuracy of slope ditching, and situation Ⅲ will also significantly increase the ditching resistance. The vertical height relationship between the FDS and RDP should be as shown in situation Ⅱ, where the bottom of both components is at the same horizontal level. The fitted equation for the relationship between the front and rear distributed soil-contacting components and traction resistance is as follows:

$$F_f = 0.017x^2 - 1.173x + 26.007 \quad (1)$$

where, F_f is the traction resistance, N; x is the distance between the front and rear soil-contacting components, cm.

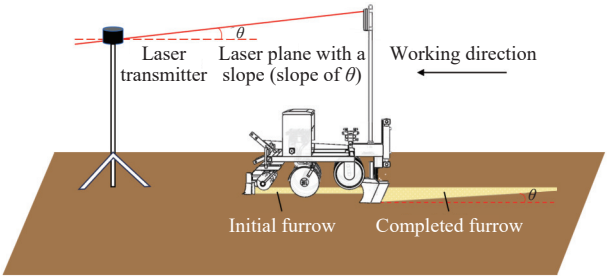

Figure 3 Working principle diagram of wheat seeder

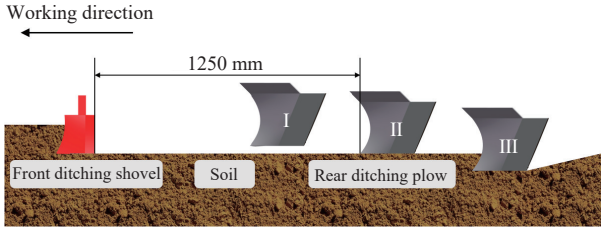

Figure 4 Schematic diagram of arrangement of FDS and RDP

According to Equation (1), when the distance between the front and rear soil-contacting components exceeds 35 cm, the traction resistance increases with the distance[27]. An analysis of the distribution and installation of the machine's components indicates that, to prevent operational obstruction or interference, the minimum distance between the FDS and the RDP should be greater than 1180 mm. Considering practical manufacturing conditions and clearance requirements, the front-to-rear installation distance between the FDS and the RDP is determined at 1250 mm.

3 Design and analysis of key components

3.1 Design of front ditching shovel

The FDS is the foremost soil-contacting component during the operation of the machine, and its function is to create the initial furrow. As shown in Figure 5, it consists of the shovel tip, shovel body, and shovel column. According to the agronomic requirements of wheat seeding in rice stubble fields and referring to the existing research[6,25], the height of the FDS is designed to be 180 mm, the maximum ditching width is 80 mm, and the shovel tip is an equilateral triangle with a side length of 60 mm.

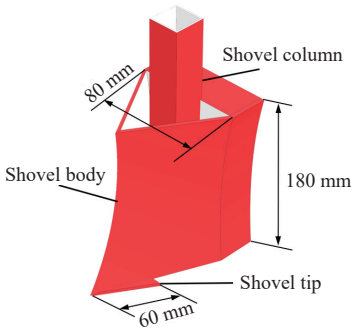

Figure 5 Front ditching shovel

3.2 Analysis of furrow soil displacement

To prevent furrow soil from accumulating on both sides of the drainage furrow, the soil deflector and spiral soil leveler are designed to transport the furrow soil generated by the FDS, as shown in Figure 6. The furrow soil flows through the deflector to the spiral soil leveler, which conveys and spreads the soil evenly onto the top surface of the ditch (the arrows in Figure 6 indicate the direction of soil movement). The backward inclination angle and downward inclination angle are two important design parameters of the soil deflector. To reduce soil blockage and ensure effective deflection, the backward inclination angle and downward inclination angle are determined to be 60° and 30°, respectively, with reference to existing research[28].

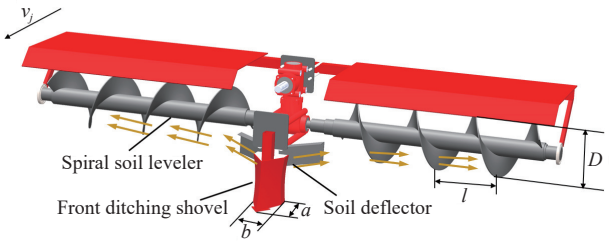

Figure 6 Soil deflector and spiral soil leveler

Under general working conditions, the penetration depth of the spiral blade into the soil is 0-3 cm. Assuming that the maximum volume of furrow soil created by the FDS per hour is M_0, all furrow soil is processed by the spiral soil leveler, and the FDS surface can be simplified as a plane, then Equation (2) is as follows:

$$M_0 = 3600\mu abS_0 v_j \tag{2}$$

where, M_0 is the maximum furrow soil volume, t/h; μ is the unit volume mass of the material, t/m³; a and b are the length and width of the FDS, respectively, m; S_0 is the maximum ditching depth of the FDS, m; v_j is the operating speed of the machine, m/s.

The soil bulk density in the typical rice-wheat rotation area was measured to be 1.69 t/m³. Assuming the operating speed of the seeder is 1.8 m/s, the maximum furrow soil volume is calculated to be 21.45 m³. Under ideal working conditions, assuming a constant rotational speed of the spiral blade and ignoring the influence of the spiral shaft diameter, then Equation (3) is as follows:

$$\begin{cases} L = 3600\mu k S_L V_h \\ S_L = \dfrac{\pi c D^2}{4} \\ V_h = \dfrac{nl}{60} \\ D \geq \psi \sqrt[\frac{5}{2}]{\dfrac{L}{km\mu}} \end{cases} \tag{3}$$

where, L is the conveying capacity, t/h; k is the inclined conveying coefficient; S_L is the cross-sectional area of the material entering the conveyor, m²; V_h is the rotational speed of the spiral blade, r/min; c is the material filling coefficient; D is the diameter of the spiral blade, m; n is the rotational speed of the spiral shaft, r/min; l is the pitch, m; ψ is the material characteristic coefficient.

Based on the working conditions and existing research, the parameters are set as k=1, c=0.5, and ψ=0.614. From Equation (3), $D \geq 0.13$ is obtained. Considering the practical manufacturing constraints, the spiral blade diameter is determined to be 0.18 m, the pitch is 0.25 m, and the spiral shaft diameter is 0.04 m. The rotational speed of the spiral shaft is a critical factor affecting the conveying capacity. From $L \geq M_0/2$, it is obtained that n>33.27 r/min. Additionally, the rotational speed of the spiral shaft should not exceed its allowable speed:

$$n \leq n_{\max} = \frac{A}{\sqrt{D}} \tag{4}$$

where, $n_{\max}$ is the allowable rotating speed of the spiral shaft, r/min; A is the comprehensive material characteristic coefficient, set to 44.2.

It can be obtained that $n_{\max}$=104.18 r/min, so the operating rotational speed range of the spiral shaft is 33.27-104.18 r/min. As the rotational speed of the spiral shaft increases, the impact of vibration on operational accuracy also intensifies. Therefore, a relatively lower value should be selected, provided that the requirements for furrow soil transportation are met.

3.3 Design of rear ditching plow

3.3.1 Structure design

Based on the initial furrow, the RDP forms a sloped furrow bottom and a complete furrow profile through soil movement and compaction. As shown in Figure 7, the RDP consists of a moldboard surface, a top plate, side plate, and a plow column. The moldboard surface breaks the soil and diverts it to both sides, the side plates compact the furrow walls, the top plate prevents soil from falling into the furrow bottom, and the plow column serves for connection and height adjustment. Based on the local wheat sowing drainage requirements and the known width of the FDS, the minimum width of the RDP is determined to be 80 mm, and the maximum width is 380 mm.

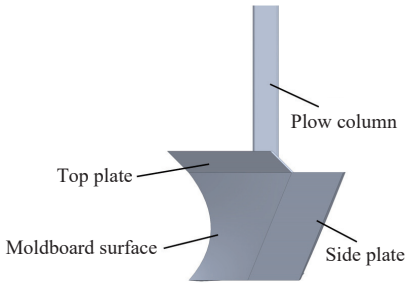

Figure 7 Rear ditching plow

3.3.2 Analysis of soil mechanics and moldboard surface design

The horizontal straight element method was used to design the moldboard surface of the RDP. During the ditching operation, the RDP moves downward to cut the soil while moving along the working direction. Simultaneously, soil particles slide obliquely rearward relative to the moldboard. The moldboard surface is an irregular spatial surface. As shown in Figure 8, a force analysis of soil particles during the operation process is performed to examine the factors affecting the ditching performance of the RDP on slopes.

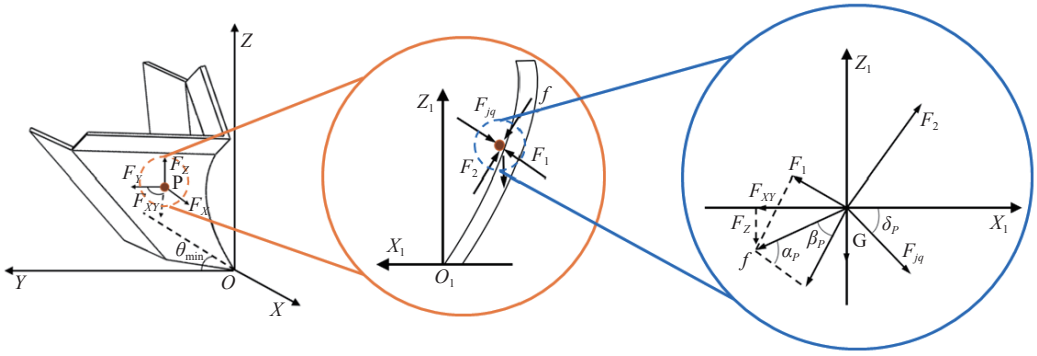

Figure 8 Force analysis of soil particle during the operation of RDP

As shown in Figure 8, a spatial rectangular coordinate system was established with the moldboard surface as the reference. The soil particle P was selected as the research object, the plow tip was set as the origin, the forward direction of the plow was defined as the *X*-axis, the vertically upward direction as the *Z*-axis, and the direction perpendicular to the *XZ*-plane as the *Y*-axis. During the operation of the RDP, without considering torque, the forces acting on the soil particle were simplified into a spatial force system consisting of mutually perpendicular forces: F_X along the *X*-axis, F_Y along the *Y*-axis, and F_Z along the *Z*-axis. The angle of the straight element and the curvature of the guiding curve vary at different points on the moldboard of the RDP. Consequently, the magnitude and direction of the support force and friction force acting on the soil clod at each point on the moldboard continuously change. A cross-section passing through point P and parallel to the *OYZ* plane was selected, and an $O_1X_1Z_1$ coordinate system was established. Further analysis is performed in this coordinate system to obtain the force equilibrium equation:

$$\begin{cases} F_1\sin\beta_P + f\cos\beta_P - F_{jq}\cos\delta_P - F_2\sin\delta_P = 0 \\ F_1\cos\beta_P + F_2\cos\delta_P - G - f\sin\alpha_P - F_{jq}\sin\delta_P = 0 \end{cases} \tag{5}$$

where, F_1 is the support force on the soil particle, N; f is the friction force on the soil particle, N; F_{jq} is the shear force on the soil particle, N; F_2 is the normal pressure on the soil particle, N; G is the gravity of the soil particle, N; β_P is the equivalent soil lifting angle, (°); and δ_P is the soil shear angle, (°).

Assuming that the operating width of the RDP is L_a, the operating depth is L_b, and the minimum element angle is θ_{min}, then Equation (6) is as follows:

$$\begin{cases} F_{jq} = \dfrac{L_aL_b}{\cos\theta_{min}\sin\delta_P}\tau_P \\ f = F_1\tan\alpha_P \\ F_H = \dfrac{F_1}{\cos\alpha_P} \\ F_{XY} = F_H\sin(\alpha_P+\beta_P) \\ F_X = F_{XY}\sin\theta_P \end{cases} \tag{6}$$

where, τ_P is the shear stress, N/m^2; θ_P is the equivalent straight element angle, (°).

According to Equations (5) and (6), the force F_X on the soil particle *P* along the *X*-axis can be obtained:

$$F_X = \frac{\sin\theta_P\sin(\alpha_P+\beta_P)\left(\tau_PL_aL_b + G\sin^2\delta_P\cos\theta_{min}\right)}{\sin\delta_P\sin(\alpha_P+\beta_P+\delta_P)\cos\theta_{min}} \tag{7}$$

The force acting on the soil particle in the *X*-axis direction has a significant impact on slope ditching. From Equation (7), it can be concluded that F_X is related to the equivalent soil-lifting angle β_P, the minimum element angle θ_{min}, and the equivalent straight element angle θ_P. Therefore, the performance of the RDP during slope ditching is significantly affected by the soil-lifting angle, the minimum element angle, and the maximum element angle.

As shown in Figure 9, the guiding curve MP consists of the straight segment MN and the curved segment NP. To ensure optimal cutting performance of the RDP, the segment NP should be a uniformly varying arc curve, approximating to a parabolic shape.

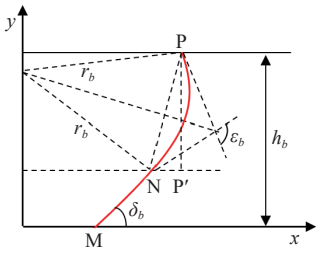

Figure 9 Guiding curve theoretical analysis

From the geometric relationship in the above figure, the following equations can be obtained:

$$\begin{cases} l_{NP} = \sqrt{l_{NP'} + l_{KK'}} = 2r_b\cos\dfrac{\varepsilon_b}{2} \\ l_{NP'} = r_b\sin(\varepsilon_b-\delta_b) - r_b\sin\delta_b \\ l_{PP'} = h_b - l_{MN}\sin\delta_b \end{cases} \tag{8}$$

$$r_b = \frac{h_b - l_{MN}\sin\delta_b}{\sqrt{\cos^2\dfrac{\varepsilon_b}{2} - [\sin(\varepsilon_b-\delta_b) - \sin\delta_b]^2}} \tag{9}$$

where, r_b is the radius of arc NP, mm; ε_b is the angle between the tangents at the two endpoints of the guiding curve, (°); δ_b is the soil-lifting angle, (°).

To improve the smoothness of the guiding curve and reduce ditching resistance, the angle between the tangents at the endpoints of the guiding curve is chosen as 135°. To enhance the soil penetration ability of the RDP during downward movement, the length of the straight segment L_{MN} is selected as 120 mm. Based on the above analysis, the range of the soil-lifting angle is determined to be 20°-50°, the range of the minimum element angle is 23°-53°, and the range of the maximum element angle is 28°-58°.

4 Determination of RDP optimal parameters by DEM

4.1 Establishment of the discrete element model

In the rice-wheat rotation area of the middle and lower Yangtze River, the alternating wet and dry conditions caused by water and drought rotation result in the soil experiencing cycles of wetting and drying. The soil moisture content is high before the wheat sowing, and there is a certain bonding force between the soil particles. The

Hertz-Mindlin with Bonding model, by generating bonding forces between particles, can effectively simulate soil discontinuity and agglomeration characteristics, thereby addressing the nonlinear interactions between agricultural tools and soil[29-31]. Under the influence of external forces, the bonds between particles are broken, resulting in fragmentation and fracture. Cheng et al.[32-34] employed this model as the contact model for soil particles in their study of soil-tool interactions in the rice-wheat rotation area of the middle and lower Yangtze River. Given its successful application in previous studies, the Hertz-Mindlin with Bonding model is also adopted in this study for modeling the contact behavior of soil particles. When the bonding stiffness is 4.8×10^{7} N/m^{3} and the critical stress is 5.5×10^{5} Pa, it better reflects the mechanical characteristics of the interaction between soil and components. The measured field soil moisture content is 33%, and the bonding radius is calculated to be 9.5 mm based on the formula. The soil bin dimensions are set to 2200 mm×1000 mm×500 mm in EDEM 2020, and spherical particles with a radius of 8 mm are selected to simulate field soil. The parameters of the simulation model are listed in Table 3[12,35-37].

Table 3 DEM parameters used in the simulations

Category	Parameter	Value
Soil	Average moisture content/%	33
	Density of soil particles/kg·m^{-3}	2100
	Poisson's ratio of soil	0.4
	Shear modulus of soil/Pa	1×10^{6}
Steel	Density of steel/kg·m^{-3}	8100
	Poisson's ratio of steel	0.3
	Shear modulus of steel/Pa	8.0×10^{10}
Soil-soil	Coefficient of friction	0.5
	Coefficient of rolling friction	0.35
	Coefficient of restitution	0.45
Soil-steel	Coefficient of friction	0.3
	Coefficient of rolling friction	0.15
	Coefficient of restitution	0.5

As shown in Figure 10, to improve simulation efficiency, the machine model was simplified by removing parts that do not affect the simulation results, while retaining the FDS, spiral leveler, and RDP. The model was saved in STEP format using SolidWorks 2022 and imported into EDEM 2020 software. In the EDEM creator module, the penetration depth of the FDS is adjusted to 20 cm, and the forward speed of all working components is set to 1 m/s. The downward movement speed of the RDP is set to 0.004 m/s, and the rotational speed of the spiral leveler is set to 60 r/min. In the EDEM simulator module, the fixed time step is set to 2×10^{-5} s, the grid cell size is set to 3 times the particle radius, and the total simulation time is 5 s.

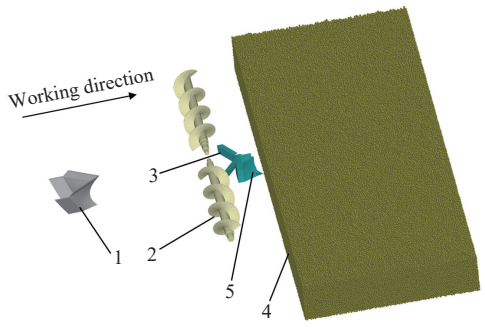

1. RDP 2. Spiral soil leveler 3. Soil deflector 4. Soil bin 5. FDS

Figure 10 Overall simulation model diagram

4.2 Test factors and evaluating indices

Through theoretical analysis and preliminary experiments, the test factors are determined to be the soil-lifting angle x_1, minimum element angle x_2, and maximum element angle x_3 of RDP. Based on the theoretical analysis results and considering the rationality of test design and manufacturing, the range of the soil-lifting angle is further determined to be 20°-50°, the range of the minimum element angle is 35°-45°, and the range of the maximum element angle is 40°-50°. To explore the optimal parameters of the three factors (soil-lifting angle, minimum element angle, and maximum element angle), a three-factor and three-level Box-Behnken test is conducted. The test factors and levels are listed in Table 4.

Table 4 Code of test factors

Code	Experimental factors		
	Soil lifting angle x_1/(°)	Minimum element angle x_2/(°)	Maximum element angle x_3/(°)
–1	20	35	40
0	35	40	45
1	50	45	50

The slope stability coefficient is used as the test index for ditching performance. As shown in Figure 11, a horizontal reference line is established directly above the soil surface, and 11 equidistant cross-sections of the soil bin are taken along the forward direction. The horizontal line at the furrow bottom is fitted using the plane coordinates of the soil particles at the bottom of the cross-sections. The distance between the horizontal bottom line and the horizontal reference line is denoted as h_j.

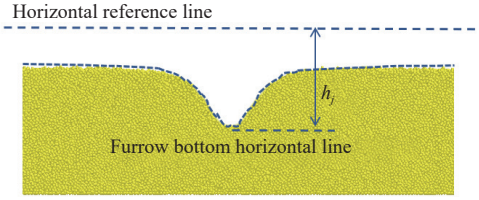

Figure 11 Test index measurement method

The distance from the first cross-section furrow bottom horizontal line to the horizontal reference line is h_0. The slope value of each cross-section furrow bottom is denoted as $D_j=h_j+h_{j-1}$. The calculation method for the slope stability coefficient is as follows:

$$\begin{cases} D_d = \left(\sum_{j=1}^{n} D_j\right) \Big/ N_1 \\ D_p = \left(1 - D_d \sqrt{\dfrac{\sum_{j=1}^{n}\left(D_j - D_d\right)^2}{N_1 - 1}}\right) \times 100\% \end{cases} \tag{10}$$

where, N_1 is the number of cross sections; D_j is the group j slope value; D_d is the average slope value; D_p is the slope stability coefficient.

4.3 Simulation process and analysis of soil particle movement

As shown in Figure 12, taking the parameter combination of soil-lifting angle 35°, minimum element angle 40°, and maximum element angle 45° as an example, the movement of soil particles during the ditching process in the simulation test is analyzed. The FDS breaks and cuts into the soil first, thus causing a greater disturbance to the soil. The soil displaced by the FDS operation, under the guidance of the soil deflector and the spiral leveler, flows

towards both sides of the furrow. The movement speed of soil particles gradually decreases, which is beneficial for surface leveling. The moldboard surface of the RDP creates a greater disturbance to the soil, and the side plate effectively prevents soil from flowing back, which helps maintain the integrity of the furrow shape.

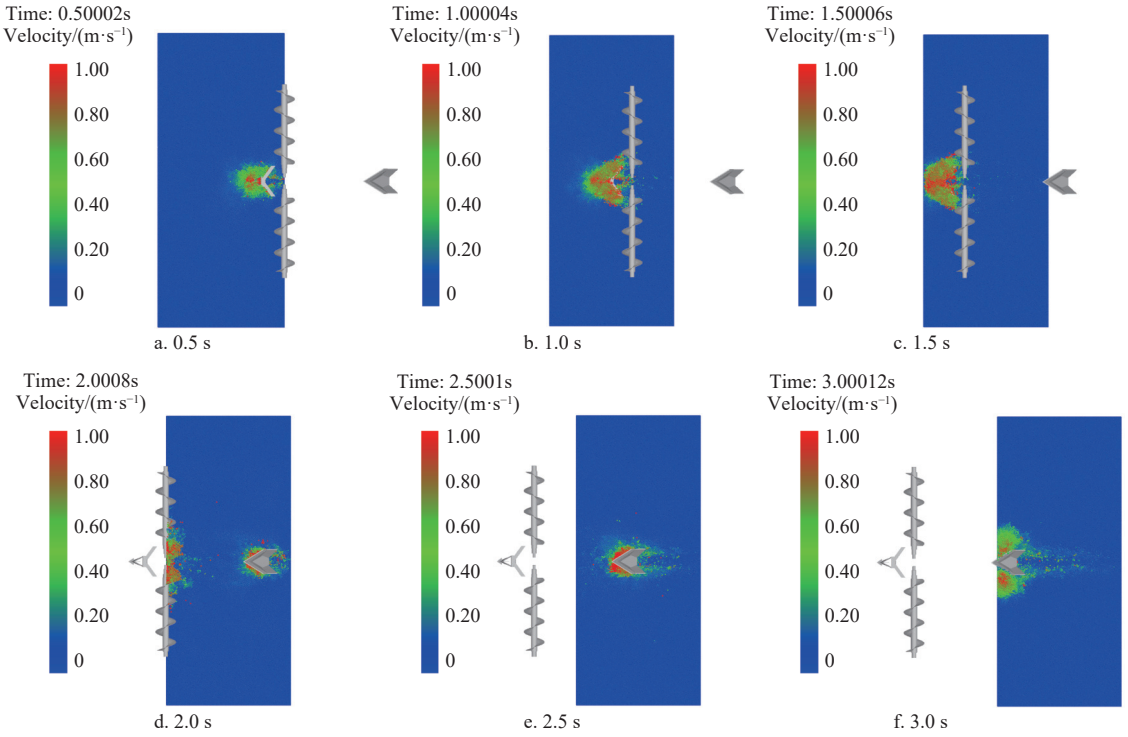

Figure 12 Simulation diagram of FDS and RDP

4.4 Simulation test results

Data from the stable stage were selected for analysis, and the test results are shown in Table 5. A quadratic regression analysis of the test results was performed using Design-Expert 8.0.6 software, and a multiple regression fitting was conducted to obtain the regression equation for the evaluation index D_p.

Table 5 Simulation test results

No.	Test factors x_1	x_2	x_3	Evaluation index D_p/%
1	–1	–1	0	88.61
2	1	–1	0	95.95
3	–1	1	0	91.92
4	1	1	0	96.01
5	–1	0	–1	88.97
6	1	0	–1	94.68
7	–1	0	1	90.91
8	1	0	1	96.03
9	0	–1	–1	92.68
10	0	1	–1	93.52
11	0	–1	1	93.46
12	0	1	1	93.88
13	0	0	0	92.63
14	0	0	0	91.98
15	0	0	0	93.46
16	0	0	0	92.74
17	0	0	0	92.25

Table 6 presents the analysis of variance (ANOVA) for the slope stability coefficient. The test results (p<0.01) indicate that the test model is significant, and the regression model is statistically meaningful. Among the main factors, the soil-lifting angle has the most significant impact on the evaluation index, followed by the minimum and maximum element angles, both of which also significantly affect the evaluation index. The order of influence of each factor on the slope stability coefficient is soil-lifting angle >minimum element angle>maximum element angle. Among the interaction terms, the soil-lifting angle and the minimum element angle have a significant impact on the evaluation index, while other interaction terms are not significant. The lack of fit p=0.4051 (p>0.1) is not significant, indicating that there is a significant quadratic relationship between the evaluation indices and test factors. The regression equation between the factors and evaluation index is as follows:

$$D_p = 61.649\,44 + 0.618\,83x_1 + 0.494\,92x_2 + 0.110\,75x_3 - 0.010\,833x_1x_2 \quad (11)$$

Table 6 Variance analysis of slope stability coefficient

Source of variation	Sum of squares	DF	Mean square	F-value	p-value
Model	71.64	9	7.96	22.78	0.0002***
x_1	61.94	1	61.94	177.29	<0.0001***
x_2	2.68	1	2.68	7.67	0.0277**
x_3	2.45	1	2.45	7.02	0.0330**
x_1x_2	2.64	1	2.64	7.56	0.0285**
x_1x_3	0.087	1	0.087	0.25	0.6330
x_2x_3	0.044	1	0.044	0.13	0.7328
x_1^2	0.054	1	0.054	0.16	0.7053
x_2^2	1.64	1	1.64	4.69	0.0670
x_3^2	0.093	1	0.093	0.27	0.6209
Lack of fit	1.18	3	0.39	1.24	0.4051
Pure error	1.27	4	0.32		
Cor total	74.09	16			

Note: *** means highly significant (p<0.01), ** means very significant (0.01< p<0.05), * means significant (0.05<p<0.1).

4.5 Response surface analysis and optimal parameter determination

The data were processed using Design-Expert 8.0.6 software, and the response surface showing the significant interaction between factors and the evaluation index was obtained. For the slope stability coefficient, the interaction effect between the soil-lifting angle and the minimum element angle is shown in Figure 13. When the minimum element angle is determined, the slope stability coefficient increases with the increase in the soil-lifting angle, and the optimal range for the soil-lifting angle is 46.21°-49.52°. When the soil-lifting angle is determined, the slope stability coefficient increases with the increase in the minimum element angle, and the optimal range for the minimum element angle is 42.09°-44.86°.

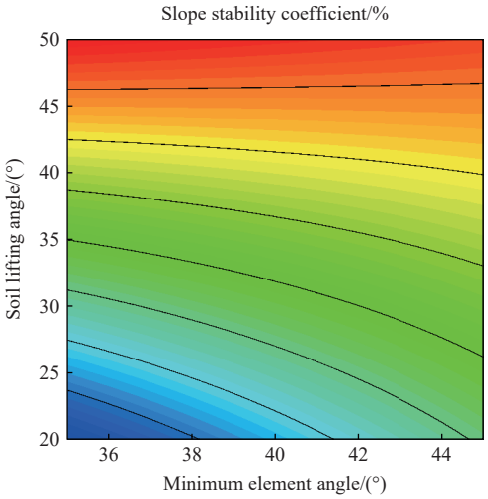

Figure 13 Response surface between soil-lifting angle and minimum element angle

To obtain the optimal structural parameters of the RDP, the regression model was optimized using the constraint objective in the optimization module of Design-Expert 8.0.6 software. The optimization constraints, objectives, and constraint functions were selected based on actual operations and related theories.

$$\begin{cases} \max D_p(x_1, x_2, x_3) \\ \text{s.t.} \begin{cases} 40^\circ \le x_1 \le 50^\circ \\ 40^\circ \le x_2 \le 45^\circ \\ 45^\circ \le x_3 \le 50^\circ \end{cases} \end{cases} \tag{12}$$

The objective function was optimized to obtain multiple optimized parameter combinations. Considering the actual manufacturing conditions, the optimal parameter combination was selected as follows: the soil-lifting angle is 50°, the minimum element angle is 35°, and the maximum element angle is 40°, with a corresponding slope stability coefficient of 95.95%.

5 Field test

5.1 Field test conditions

The field test was conducted in October 2023 at the Mechanized Production Demonstration Test Field in Shandong Province (115°48′49.82″E, 35°25′11.89″N), as shown in Figure 14. The test plot was treated with rotary tillage and the overall soil conditions were consistent with the characteristics of high-moisture soil typically found in rice-wheat rotation areas in China. The average soil moisture content within the 0-400 mm soil layer was 33.17%, the soil bulk density was 1.61 g/cm^3, and the average soil compactness was 693.58 kPa. The operating speed of the tractor was 1 m/s, and the length of the straight operating section was 40 m, with the middle 33 m selected as the data measurement section. Eleven measurement points were selected at equal intervals, with the first measurement point serving as the reference point. The other measurement points were sequentially numbered, and each experimental group was repeated three times.

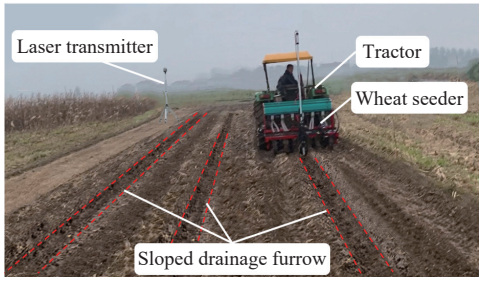

Figure 14 Field operation

5.2 Surveying and mapping of drainage furrow cross-section

As shown in Figure 15, the laser orthogonal measurement method was used to survey and map the drainage furrow cross-section at the measurement point. The laser transmitter was placed on the ground, and two positioning rods were placed vertically on both sides of the furrow surface at the measurement point. Adjustable scale rulers were fixed on the positioning rods as the horizontal measurement reference. The vertical positions of the scale rulers were determined by the laser transmitter, ensuring that the measurement reference remained horizontal. When surveying and mapping the drainage furrow cross-section, the center of the furrow was used as the vertical distance reference. The vertical distance between the horizontal reference and the furrow bottom, as well as the furrow walls, were measured and recorded at 20-mm intervals on both sides. When surveying and mapping the plane shape on both sides of the drainage furrow, the same method was

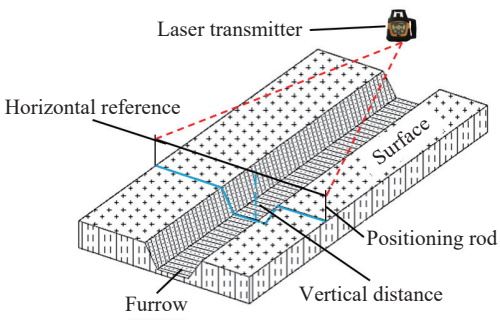

a. Schematic diagram of measurement method

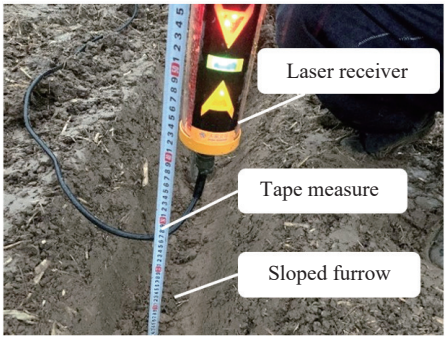

b. Data measurements

Figure 15 Surveying and mapping of drainage furrow cross-section

applied to measure and record the distance between the horizontal reference and the furrow surface at 100-mm intervals. The above measurement data were processed using Excel software to generate cross-section diagrams.

5.3 Field test indices

Currently, the performance evaluation indices of the combined sowing and ditching machine mainly include furrow dimensions and the stability coefficient, but the evaluation objects are limited to level furrows. Since the furrows formed by the machine in this study have a slope, the furrow shape will change due to the ditching slope. Based on the actual conditions observed in the field pre-tests, the slope stability coefficient and slope accuracy coefficient are determined as the test indices for the ditching operation. The calculation methods of the slope stability coefficient and slope accuracy coefficient are as follows:

$$\begin{cases} \bar{P} = \dfrac{\sum_{j=1}^{N} P_j}{N_2} \\ \sigma_P = \sqrt{\dfrac{\sum_{j=1}^{N} \left(P_j - \bar{P}\right)^2}{N_2 - 1}} \\ U_P = \left(1 - \dfrac{\sigma_P}{\bar{P}}\right) \times 100\% \end{cases} \tag{13}$$

where, P_j is the slope value of the measurement point; $\bar{P}$ is the average slope value; σ_P is the standard deviation of slope value; U_P is the slope stability coefficient; N_2 is the number of measurement points, N_2=10.

$$\begin{cases} \sigma'_P = \sqrt{\dfrac{\sum_{j=1}^{N} \left(P'_j - P_0\right)^2}{N_2 - 1}} \\ U'_P = \left(1 - \dfrac{\sigma'_P}{P_0}\right) \times 100\% \end{cases} \tag{14}$$

where, P'_j is the slope value of the measurement point; P_0 is the slope value of the laser plane; σ'_P is the relative slope standard deviation; U'_P is the slope accuracy coefficient.

5.4 Results and discussion

Three different furrowing slopes are set. The furrowing slope corresponding to Group A is the slope with a height difference of 30 cm in a plot with a length of 50 m; the furrowing slope corresponding to Group B is the slope with a height difference of 20 cm in a plot with a length of 50 m; and the furrowing slope corresponding to Group C is the slope with a height difference of 10 cm in a plot with a length of 50 m. Under three different slope values, the furrowing device can create trapezoidal drainage furrows with obvious slope, which is conducive to the drainage of field ponding. The field test results are shown in Figure 16.

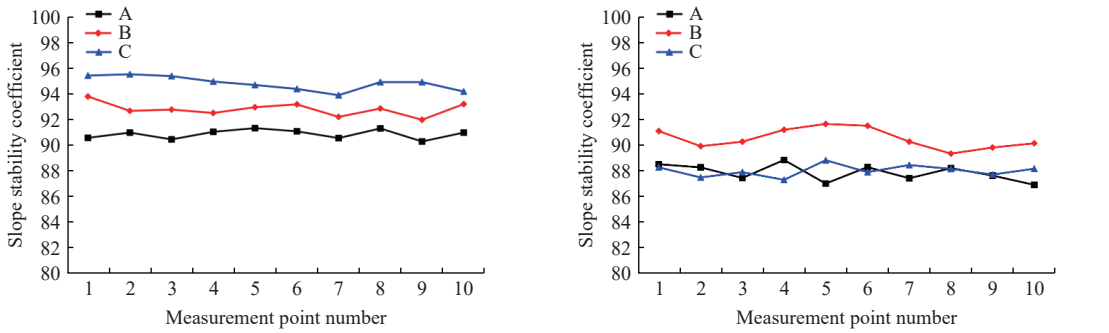

a. The slope stability coefficient of different measurement point b. The slope accuracy coefficient of differentmeasurement point

Figure 16 Field test results

As shown in Figure 16, as the slope value increases, the slope stability coefficient decreases. However, the slope stability coefficient under all three slope settings is greater than 85%, which meets the operational standards for wheat sowing and drainage ditching. Under the three slope settings, the slope accuracy coefficient of the ditching device is also greater than 85%. Group B exhibits the highest accuracy coefficient, likely because the furrow depth in Group B is within the optimal working depth range for the device.

The cross-section of the drainage furrow in Group B is presented in Figure 17. To enhance the clarity of the cross-section curve in the figure, measurement points 2, 4, 6, 8, and 10 are selected to display, corresponding to line a, b, c, d, and e in the figure. The cross-section of the drainage furrow is trapezoidal, with varying furrow depths at different measurement points, forming a sloped drainage furrow. Both sides of the furrow are relatively flat.

The slope stability coefficient reflects the operational performance of the ditching device, while the slope accuracy coefficient represents the deviation between the actual operation and the set value, both of which have a significant influence on the drainage effect of the furrow. A slope stability coefficient greater than 89% indicates that the furrowing device has better operational stability. A low slope stability coefficient may lead to furrow deformation, thereby affecting drainage efficiency. The reduction in the slope accuracy coefficient can be attributed to several factors. First, machine vibration plays a critical role in affecting slope accuracy, particularly when operating on uneven terrain. Such vibrations can induce instability in the measurement data, resulting in systematic errors. Second, errors in the laser transmission and reception process may also affect slope accuracy. In complex field environments, laser signals may experience interference or attenuation, leading to measurement discrepancies.

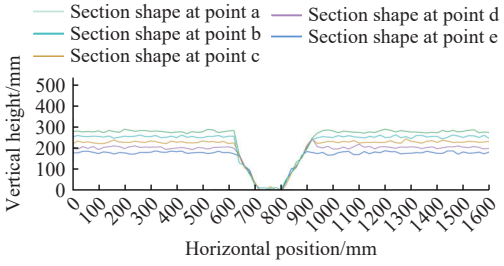

Figure 17 Mapping diagram of sloped furrow cross-section in group B test

In comparison to the simulation results, the slope stability coefficient in the field tests is lower, and this discrepancy can be attributed to the complexity and variability of the field environment. Field tests are conducted under natural conditions, where factors such as soil moisture content, terrain slope variations, and dynamic machine responses may all influence ditching accuracy. In contrast, simulation tests are typically conducted under idealized conditions, assuming uniform soil properties, stable operating environments, and optimal machine performance. Consequently, simulation results are generally more idealized than those observed in field tests. In the rice-planting areas of the middle and lower Yangtze River, the furrow-ditching operation for sowing wheat or rapeseed is typically carried out using either active or passive methods. The passive furrow-ditching device is characterized by a simple structure; however, it exhibits relatively poor operational stability and limited soil fragmentation capabilities. The active furrow-ditching device is suitable for high-speed operations and can effectively fragment the soil, but it generates significant vibrations. This study employs a laser alignment system to achieve precise slope ditching, making the use of active rotary ditching unsuitable. Compared to existing passive furrow-ditching devices, although there is no significant improvement in ditching stability, the proposed method can effectively create sloped drainage furrows, thereby significantly improving the drainage of field waterlogging.

6 Conclusions

This paper designed a rear ditching plow, which can be combined with the front ditching shovel to create a sloped drainage furrow. The working principle of the front shovel and rear plow combination ditching device was explained, and the relative positional relationship between the FDS and RDP on the wheat seeder was determined. Through force analysis, the main factors affecting the operational performance of the RDP were identified as the soil-lifting angle, the minimum element angle, and the maximum element angle, and the value ranges were determined.

The discrete element method was used to study the effect of different structural parameter combinations of the RDP on slope stability. Through parameter optimization, the optimal parameter combination was determined, with a soil-lifting angle of 50°, a minimum element angle of 35°, a maximum element angle of 40°, and a slope stability coefficient of 95.95%.

The optimal parameter combination obtained from the simulation was used to manufacture the ditching components, which were then installed on the wheat seeder for field tests. The test results show that the ditching device can effectively create sloped trapezoidal drainage furrows, with both the slope stability coefficient and slope accuracy coefficient exceeding 85%, meeting the local agronomic planting requirements and improving the drainage effect during wheat sowing in rice-stubble fields.

Acknowledgements

This research was funded by the China Agriculture Research System of MOF and MARA (Grant No. CARS-03), and was supported by the 2115 Talent Development Program of China Agricultural University.

[References]

[1] Yuan G Y, Huan W W, Song H, Lu D J, Chen X Q, Wang H Y, et al. Effects of straw incorporation and potassium fertilizer on crop yields, soil organic carbon, and active carbon in the rice-wheat system. Soil and Tillage Research, 2021; 209: 104958.

[2] Luo H P, Zou N, Hu X Y, Wang S N. Climatic potential productivity and resources utilization efficiency of major grain crops in the main grain production areas of China, 1980-2019. Resources Science, 2021; 43(6): 1234–1247. (in Chinese)

[3] He H, Li D D, Wu Z, Zhang T C, Pan F F, Yang S Y. Effects of drainage on N_2O emission and yield of rice-wheat rotation system in the middle and lower reaches of the Yangtze River. Journal of Anhui Agricultural University, 2022; 49(4): 652–658. (in Chinese)

[4] Qin K, Ding W M, Fang Z C, Du T T, Zhao S Q, Wang Z. Design and experiment of seeding system for harvest ditch and stalk-disposing machine. Transactions of the CSAM, 2017; 48(5): 54–62. (in Chinese)

[5] Zhu H B, Li H W, He J, Wang Q J, Li H, Lu C Y. No-till wheat seeder with two-axel drive anti-blocking in rice stubble field. Transactions of CSAM, 2013; 44(6): 39–44. (in Chinese)

[6] Hu H, Li H W, Li C Y, Wang Q J, He J, Li W Y, et al. Design and experiment of broad width and precision minimal tillage wheat planter in rice stubble field. Transactions of CSAE, 2016; 32(4): 24–32. (in Chinese)

[7] Zheng K, Liu G Y, Guo L W, Cheng J, Xia J F, Li Y F. Design and experiment of wide-boundary seldom-tillage wheat planter with soil-shunting function. Transactions of the CSAM, 2022; 53(2): 128–138. (in Chinese)

[8] Liao Y T, Wu A Y, Qin Y H, Liao Q X, Ou Y H, Zhang Q S, et al. Design and experiment of convex ridge surface shaping device for rapeseed direct seeding. Transactions of the CSAM, 2024; 55(12): 121–133. (in Chinese)

[9] Liu X P, Xiao W L, Ma L, Liu L C, Wan G W, Liao Q X. Design and ditching quality experiment on combined ship type opener of direct rapeseed seeder. Transactions of the CSAM, 2017; 48(11): 79–87. (in Chinese)

[10] Liu L C. Ditching device design and soil surface quality study of no-tillage direct seeder for rapeseed. PhD dissertation. Hubei: Huazhong Agricultural University, 2019. 166p. (in Chinese)

[11] Zhang Q S, Qi T, Ao Q, Shu C X, Liao Y T, Liao Q X. Design and experiment of rapeseed direct seeding machine with furrow opener and shallow plowing. Transactions of the CSAM, 2023; 54(10): 58–67, 104 (in Chinese)

[12] Wang L Z, Liao Q X, Li M L, Shan Y Y, Li X R, Zhang Q S, et al. Drive-type ditching device of the high-speed no-tillage direct seeder for rapeseed. Transactions of CSAE, 2023; 39(19): 15–26. (in Chinese)

[13] Wang Y S, Li C J, Chen J, Hu H T, Shi L G, Zhu D H, et al. Preliminary effects of laser land leveling and precision seeding on winter wheat production and soil physicochemical properties. Journal of Irrigation and Drainage, 2016; 35(S1): 37–40. (in Chinese)

[14] Jat M L, Gathala M K, Ladha J K, Saharawat Y S, Jat A S, Kumar V, et al. Evaluation of precision land leveling and double zero-till systems in the rice-wheat rotation: Water use, productivity, profitability and soil physical properties. Soil and Tillage Research, 2009; 105(1): 112–121.

[15] Chen J M, Zhao Z X, Chen J Q, Yu L, Ye J. Design of nonlinear leveling control system for paddy land leveler. Transactions of the CSAM, 2014; 45(7): 79–84. (in Chinese)

[16] Tang L M, Hu L, Zang Y, Luo X W, Zhou H, Zhao R M, et al. Method and experiment for height measurement of scraper with water surface as benchmark in paddy field. Computers and Electronics in Agriculture, 2018; 152: 198–205.

[17] İrsel G, Altinbalik M T. Adaptation of tilt adjustment and tracking force automation system on a laser-controlled land leveling machine. Computers and Electronics in Agriculture, 2018; 150: 374–386.

[18] Hu L, Du P, Luo X W, Zhou H, Tang L M, Su H Y. Design and experiment on multi-wheel support laser land leveler hanging on tractor. Transactions of the CSAM, 2019; 50(8): 15–21. (in Chinese)

[19] Zhang L C, Yang W, Li Z X, Cai C F, Wang T W. Quantification of soil surface roughness during soil erosion using laser micro-topographical scanner. Transactions of the CSAE, 2014; 30(22): 155–162. (in Chinese)

[20] Wang W W, Li J, Wang Q Q, Li Z D, Wu Y Y, Chen L Q. Design and experiment for tillage soil groove measurement system. Transactions of the CSAM, 2019; 50(7): 93–99. (in Chinese)

[21] Wang S, Yi S J, Zhao B, Li Y F, Tao G X, Mao X. High-speed no-till seeder seeding depth monitoring system based on IWHO-EKF. Transactions of the CSAM, 2024; 55(3): 75–84. (in Chinese)

[22] Sauders C, Ucgul M, Godwin R J. Discrete element method (DEM) simulation to improve performance of a mouldboard skimmer. Soil and Tillage Research, 2021; 205: 104764.

[23] Kim Y S, Siddique M A A, Kim W S, Kim Y J, Lee D K, Hwang S J, et al.

DEM simulation for draft force prediction of moldboard plow according to the tillage depth in cohesive soil. Computers and Electronics in Agriculture, 2021; 189: 106368.

[24] Zhang Q S, Liao Q X, Ji W F, Liu H B, Zhou Y, Xiao W L. Surface optimization and experiment on ditch plow of direct rapeseed seeder. Transactions of the CSAM, 2015; 46(1): 53–59. (in Chinese)

[25] Liu X P, Zhang Q S, Liu L C, Wei G L, Xiao W L, Liao Q X. Surface optimization of ship type ditching system based on differential geometry and EDEM simulation. Transactions of the CSAM, 2019; 50(8): 59–69. (in Chinese)

[26] Wang L Z, Liao Q X, Zhang Z L, Li M L, Zhang Q S, Wang L, et al. Optimization and experiments of the blade group of ditching devices in rapeseed direct seeder. Transactions of the CSAE, 2024; 40(3): 37–49. (in Chinese)

[27] Zhao Y Z, Yang Y, Zhang C G, Qi G Y, LiU L. Effect of the configuration parameters of the layered subsoiling shovel type on the draft resistance. Journal of Northeast Agricultural University, 2016; 47(2): 102–108. (in Chinese)

[28] Yang Q L, Li H W, He J, Lu C Y, Wang Y B, Wang Q J. Design and experiment of layered deep fertilization device of different fertilizers based on pneumatic distribution. Transactions of the CSAM, 2021; 52(10): 61–73. (in Chinese)

[29] Zhu Y H, Xia J F, Zeng R, Zheng K, Du J, Liu Z Y. Prediction model of rotary tillage power consumption in paddy stubble field based on discrete element method. Transactions of the CSAM, 2020; 51(10): 42–50 (in Chinese)

[30] Zou L L, Yan D W, Niu Z R, Yuan J, Cheng H, Zheng H. Parametric analysis and numerical optimisation of spinach root vibration shovel cutting using discrete element method. Computers and Electronics in Agriculture, 2023; 212: 108138.

[31] Liu W R, Zhang G Z, Wang H C, Liu H P, Kang Q X, Zhao Z Z, et al. Microscopic deformation and fragmentation energy consumption characteristics of soils with various moisture contents using discrete element method. Soil and Tillage Research, 2024; 241: 106131.

[32] Cheng J, Xia J F, Zheng K, Liu G Y, Wei Y S, Liu Z Y, et al. Construction and analysis of a discrete element model for calculating friction resistance of the typical rotary blades. Computers and Electronics in Agriculture, 2023; 212: 108303.

[33] Wang L, Bian Q W, Liao Q X, Wang B, Liao Y T, Zhang Q S. Burying stubble and anti-blocking deep fertilization composite device for rapeseed direct planting in high stubble and heavy soil rice stubble field. Transactions of the CSAM, 2023; 54(2): 83–94 (in Chinese)

[34] Liao Q X, Lin J X, Zhang Q S, Xie H M, Du W B, Wu C. Design and experiment of shovel type seedbed preparation machine suitable for rapeseed direct seeding. Transactions of the CSAM, 2022; 53(10): 26–35 (in Chinese)

[35] Ding Q S, Ren J, Adam B E, Zhao J K, Ge S Y, Li Y. DEM Analysis of Subsoiling Process in Wet Clayey Paddy Soil. Transactions of the CSAM, 2017; 48(3): 38–48. (in Chinese)

[36] Xiang W, Wu M L, Lü J N, Quan W, Ma L, Liu J J. Calibration of simulation physical parameters of clay loam based on soil accumulation test. Transactions of the CSAE, 2019; 35(12): 116–123. (in Chinese)

[37] Zhu H B, Wu X, Bai L Z, Qian C, Zhao H R, Li H. Development of the biaxial stubble breaking no-tillage device for rice stubble field based on EDEM-ADAMS simulation. Transactions of the CSAE, 2022; 38(19): 10–22. (in Chinese)